THE ASTROPHYSICAL JOURNAL, 522:1022–1036, 1999 September 10

A COMPLETE SET OF SOLUTIONS FOR CAUSTIC CROSSING BINARY MICROLENSING EVENTS

M. D. ALBROW,[1] J.-P. BEAULIEU,[2] J. A. R. CALDWELL,[3] D. L. DEPOY,[4] M. DOMINIK,[2] B. S. GAUDI,[4] A. GOULD,[4] J. GREENHILL,[5] K. HILL,[5] S. KANE,[5,6] R. MARTIN,[7] J. MENZIES,[3] R. M. NABER,[2] R. W. POGGE,[4] K. R. POLLARD,[1] P. D. SACKETT,[2] K. C. SAHU,[6] P. VERMAAK,[3] R. WATSON,[5] AND A. WILLIAMS,[7]
(THE PLANET COLLABORATION)
Received 1999 March 1; accepted 1999 April 19

ABSTRACT

We present a method to analyze binary lens microlensing light curves with one well-sampled fold caustic crossing. In general, the surface of χ^2 shows extremely complicated behavior over the nine-parameter space that characterizes binary lenses. This makes it difficult to systematically search the space and verify that a given local minimum is a global minimum. We show that for events with well-monitored caustics, the caustic crossing region can be isolated from the rest of the light curve and easily fitted to a five-parameter function. Four of these caustic crossing parameters can then be used to constrain the search in the larger nine-parameter space. This allows a systematic search for all solutions and thus identification of all local minima. We illustrate this technique using the PLANET data for MACHO 98-SMC-1, an excellent and publicly available caustic crossing data set. We show that a very broad range of parameter combinations are compatible with the PLANET data set, demonstrating that observations of binary lens light curves with a sampling of only one caustic crossing do not yield unique solutions. The corollary to this is that the time of the second caustic crossing cannot be reliably predicted on the basis of early data including the first caustic crossing alone. We investigate the requirements for determination of a unique solution and find that occasional observations of the first caustic crossing may be sufficient to derive a complete solution.

Subject headings: astrometry — dark matter — gravitational lensing

1. INTRODUCTION

Binary lens microlensing events, especially those with caustic crossings, have a number of potentially important applications. First, if the caustic crossing is well sampled, the proper motion of the lens relative to the observer-source line of sight can be measured. Since different populations have different proper motion distributions, such a measurement can help determine the nature of the lens. For example, five groups observed the event MACHO 98-SMC-1 found by the MACHO collaboration (Alcock et al. 1999) in observations toward the Small Magellanic Cloud (SMC), and all concluded that its proper motion is consistent with the lens being in the SMC rather than the Galactic halo (Afonso et al. 1998 [EROS]; Albrow et al. 1999a [PLANET]; Alcock et al. 1999 [MACHO]; Udalski et al. 1998 [OGLE]; Rhie et al. 1999 [MPS]). This provides an important clue regarding the controversy (e.g., Sahu 1994; Gould 1995) over the location and nature of the lenses currently being discovered toward the Magellanic Clouds (Aubourg et al. 1993; Alcock et al. 1997a). Second, caustic crossing binaries are one of the few classes of microlensing events for which it is possible, at least in principle, to obtain a complete solution of the mass, distance, and velocity of the lens (Hardy & Walker 1995; Gould & Andronov 1999). Third, caustic crossing events (both binary and points lens) can be used to measure the limb-darkened profile of the source star (Albrow et al. 1999b). Fourth, binary lens events can potentially tell us about the distributions of binary mass ratios and separations. The light-curve solution directly yields the mass ratio and also gives the projected separation in units of the Einstein ring. By calibrating the binary lens detection efficiency (Gaudi & Sackett 1999), the observed distribution can be compared with that predicted for various models. Finally, planet-star systems are, from a microlensing standpoint, extreme mass-ratio binaries and hence can be discovered by looking for binary lens–type events (Mao & Paczyński 1991).

For most of these applications, one must correctly and uniquely measure the parameters that describe the observed binary lens and quantify the uncertainties in this solution. Or, if an unambiguous determination is not possible, one must at least find the entire set of degenerate solutions. Note that in this paper we will use the term "solution" as a shorthand to refer to any set of parameters whose χ^2 is acceptably close to the absolute minimum χ^2 over the entire parameter space. Such "solutions" may be separable into a discrete set of local minima, or they may form a continuous subset that winds its way across parameter space. The first case is what one ordinarily imagines when one hears the term "solutions," but for brevity we will use the same term for both situations.

Nine parameters are required to specify the most basic caustic crossing binary lens event. These are usually taken to be t_0, u_0, t_E, q, d, α, ρ_*, F_s, and F_b. Here t_0 is the time of closest approach to the origin of the binary, t_E is the Ein-

[1] University of Canterbury, Department of Physics and Astronomy, Private Bag 4800, Christchurch, New Zealand.
[2] Kapteyn Astronomical Institute, Postbus 800, 9700 AV Groningen, The Netherlands.
[3] South African Astronomical Observatory, P.O. Box 9, Observatory 7935, South Africa.
[4] Ohio State University, Department of Astronomy, Columbus, OH 43210.
[5] University of Tasmania, Physics Department, G.P.O. 252C, Hobart, Tasmania 7001, Australia.
[6] Space Telescope Science Institute, 3700 San Martin Drive, Baltimore, MD 21218.
[7] Perth Observatory, Walnut Road, Bickley, Perth 6076, Australia.

stein crossing time, and u_0 is the angular impact parameter at time t_0 in units of the angular Einstein radius, θ_E,

$$\theta_E = \left(\frac{4GMD_{LS}}{c^2 D_L D_S}\right)^{1/2}, \quad (1)$$

D_L, D_S, and D_{LS} are the observer-lens, observer-source, and lens-source distances, and the mass M is the total mass of the binary. Note that $\theta_E = \mu t_E$, where μ is the proper motion. The three parameters specific to the binary character of the lens are the mass ratio $q = M_2/M_1$ of the secondary to the primary ($0 < q \leq 1$), the projected angular binary separation d in units of θ_E, and the angle α ($0 \leq \alpha < 2\pi$) between the binary separation vector (M_2 to M_1) and the proper motion of the source relative to the origin of the binary. Our convention is that the center of the binary lies on the right-hand side of the moving source, and we adopt the midpoint of the lenses as the origin of the binary. The angular size of the source in units of θ_E is ρ_*, the source flux is F_s, and F_b is the light from any unlensed sources (including the lens) that enters the aperture. If the event is observed from more than one observatory, then two additional parameters are required for each additional observatory to account for the different fluxes and backgrounds registered by different telescopes. One may include more than these basic parameters to account for other higher order effects, such as limb darkening of the source, orbital motion of the binary, and parallax effects due to the motion of the Earth, but we will ignore these effects in this paper. This means that we will be implicitly assuming that the source can be approximated as uniform.

We refer to the above parameterization as "standard" throughout this paper. However, another widely used parameterization places the binary center of mass at the origin rather than the midpoint of the binary components. In Appendix A we present explicit transformations between these two "standard" parameterizations.

Using the standard parameterization, fitting binary lens light curves poses a significant challenge for several reasons. First, χ^2 is very sensitive to small changes in most of the parameters and furthermore responds in a complicated manner. The sheer size of parameter space combined with the sensitivity of χ^2 to subtle changes in the parameters makes brute force searches practically impossible. Second, choosing suitable initial guesses for possible solutions is difficult because most of the parameters have no direct relationship to observable features in the light curve. Thus, even if one finds a trial solution, it is difficult to be sure that all possible solutions have been found. Finally, the magnification of a binary lens is nonanalytic. While this poses no significant challenge for calculating light curves for events that can be approximated as having a point source, such as binary lens events with no caustic crossings, finite-source caustic crossing light curves are notoriously difficult to calculate. Although many efficient and robust methods have been proposed to do this (Kayser & Schramm 1988; Gould & Gaucherel 1997; Bennett & Rhie 1996; Wambsganss 1997; Dominik 1998), they are invariably time consuming. This is a serious detriment to fitting a light curve because of the large number of models that must be calculated.

Mao & Di Stefano (1995) attacked the problem of fitting binary lens light curves by developing a densely sampled library of point-source binary microlensing events, each of which is characterized by cataloged "features" such as the number of maxima, heights of peaks, time between peaks, etc. They can then examine individual events, characterize their "features," and search their library for events that are consistent with these features. This alleviates many of the problems discussed above, as it reduces the search to a relatively few regions of parameter space. Mao & Di Stefano (1995) report that their method is robust for caustic crossing events since these have well-defined features. However, this method does have some shortcomings that make it difficult to apply to well-sampled caustic crossing binary lens events. First, the method relies on the approximate magnification of the observed peaks to reduce the possible space of solutions. However, the magnification of the observed peaks depends on the baseline magnitude, which can be unknown or poorly determined. Furthermore, even if the baseline is exactly measured, the magnification is not a direct observable, as it depends not only on the binary model and trajectory, but also on the amount of blended light, F_b. Finally, the peak magnification also depends on the unknown size of the source ρ_*. While it may be possible to extend the method of Mao & Di Stefano (1995) to take these difficulties into account, the search space would increase by two dimensions and thus the efficiency would decrease. Di Stefano & Perna (1997) suggested that binary lenses could be fitted by decomposing the observed light curve into a linear combination of basis functions. The coefficients of these functions could then be compared with those fitted to a library of events in order to isolate viable regions of parameter space. This is essentially the same method as Mao & Di Stefano (1995), except that rather than using gross features to identify similar light curves, one uses the coefficients of the polynomial expansion, which is more quantitative and presumably more robust. However, this method has the same shortcomings as that of Mao & Di Stefano (1995) for the same reasons. Also, the method of Di Stefano & Perna (1997) requires that, before the basis function fitting, one map the observed light curve onto the same temporal interval for which the event library light curves were fitted. This is impossible to do for only partially sampled events, or events where the fraction of blended light is unknown.

Here we propose an alternate method to systematically search for solutions in the specific case of a binary lens with one well-sampled caustic crossing. Initially, binary lens events were monitored only by the primary search groups and so were observed only once or twice per night. Since caustic crossings generally take less than 1 day, this implied that the crossings were not well sampled. For example, the first binary lens event with caustic crossings, OGLE-7, was observed by OGLE only once near the first caustic and not at all near the second (Udalski et al. 1994), although MACHO did serendipitously observe one point on the second crossing of this event thereby resolving the source (Mao et al. 1994). Dominik (1999a) showed that a large variety of binary lens parameters are consistent with the photometric data for this event as well as for another caustic crossing binary, DUO-2.

However, at present the three primary search groups, OGLE, MACHO, and EROS, all have alert systems by which they can recognize microlensing events in real time. Three other groups, GMAN (Alcock et al. 1997b), PLANET, and MPS then monitor these alerted events much more frequently. Once a source crosses the first caustic, it is possible to predict the second crossing at least a

day in advance on the basis of these frequent follow-up observations by observing the rise to the crossing (although it is not possible to predict the second caustic crossing from observations of the first alone, as we demonstrate in § 4.2). The second caustic crossing can then be observed very intensively. Indeed, one caustic crossing was even observed spectroscopically by making use of target-of-opportunity time (Lennon et al. 1996). Thus, well-sampled caustic crossings should become more common in the future.

We present our method for searching for binary lens solutions in § 2. In §§ 3 and 4 we illustrate the method using PLANET data for MACHO 98-SMC-1. We show that a broad range of parameter combinations are consistent with the PLANET data. In § 5 we therefore examine what sort of data are required to break these degeneracies.

We emphasize that our treatment of MACHO 98-SMC-1 is not intended to be definitive, but merely illustrative. A thorough investigation of this event will be made by Afonso et al. (1999) by combining data from all five groups.

2. THE METHOD

We assume that the binary lens light curve can be decomposed into two parts. The first part characterizes the caustic crossing itself and is described by a five-parameter semianalytic function. The five parameters are not directly related to any of the traditional parameters but are more directly related to observables, so that χ^2 is less sensitive to small changes in these parameters. Furthermore, the function is semianalytic and thus very simple and quick to compute. We fit the data near the caustic crossing to this function. Four of the five parameters extracted from the fit, along with a measurement of the baseline, are then used to constrain the search of parameter space. We then search for fits to the non–caustic crossing light-curve data in this restricted space. We calculate the magnification of these images from the full binary lens equation with the standard parameters. Since the magnification arising from the diverging images associated with the caustic is not being considered, χ^2 behaves much more sensibly. Furthermore, no finite-source effects need be considered when fitting to the non–caustic crossing data, greatly improving the computational efficiency of the search. The end result of this search is a complete set of trial solutions. We then perform refined searches beginning with these trial solutions, incorporating all the data, and using a variant of the method just described.

In § 2.1 we describe in detail the method of fitting and extracting parameters from the five-parameter function that describes generic caustic crossings. Section 2.2 then describes how the parameters extracted from the caustic crossing fit can be used to constrain the search for the global fit to the remaining data and an effective method for performing this search. Figure 1 is a flowchart which illustrates the relations among the various steps of the method.

2.1. *Parameterized Fit to the Caustic Crossing Data*

Imagine a point at the center of a source as it crosses a caustic. While inside the caustic, the point source has five images. As it crosses the caustic, the magnifications of two of these images diverge toward a square root singularity, until the images suddenly disappear. If we neglect any changes of the lens properties in the neighborhood of the caustic crossing, then the magnification of these two divergent images can be written (e.g., Schneider & Weiss 1986a)

$$A^0_{\rm div}(\boldsymbol{u}) = \left(\frac{\Delta u_\perp}{u_r}\right)^{-1/2} \Theta(\Delta u_\perp) \,, \tag{2}$$

where

$$\Delta u_\perp \equiv \Delta \boldsymbol{u} \cdot \boldsymbol{n}_{\rm cc} \,, \quad \Delta \boldsymbol{u} \equiv \boldsymbol{u} - \boldsymbol{u}_{\rm cc} \,, \tag{3}$$

$\boldsymbol{u}_{\rm cc}$ is the position of the caustic crossing, $\boldsymbol{n}_{\rm cc}$ is the unit vector at $\boldsymbol{u}_{\rm cc}$ pointing inward normal to the caustic, Θ is a step function, and u_r is the characteristic rise length of the caustic. The other three images are unaffected by the caustic crossing, so their total magnification can be Taylor expanded:

$$A^0_{\rm nondiv}(\boldsymbol{u}) = A_{\rm cc} + \boldsymbol{Z} \cdot \Delta \boldsymbol{u} \,, \tag{4}$$

where $A_{\rm cc}$ is the magnification of the three images at the caustic crossing and $\boldsymbol{Z}$ is the gradient of the magnification with respect to $\boldsymbol{u}$. Hence the full magnification in the neighborhood of the caustic crossing can be approximated as

$$A^0(\boldsymbol{u}) = \left(\frac{\Delta u_\perp}{u_r}\right)^{-1/2} \Theta(\Delta u_\perp) + A_{\rm cc} + \boldsymbol{Z} \cdot \Delta \boldsymbol{u} \,. \tag{5}$$

For an extended source of angular radius $\theta_* \equiv \rho_* \theta_{\rm E}$, the magnification is given by the convolution of A^0 with the source surface brightness profile, which yields (e.g., Schneider, Ehlers, & Falco 1992, pp. 215–216)

$$A(\boldsymbol{u}) = \left(\frac{u_r}{\rho_*}\right)^{1/2} G\left(-\frac{\Delta u_\perp}{\rho_*}\right) + A_{\rm cc} + \boldsymbol{Z} \cdot \Delta \boldsymbol{u} \,. \tag{6}$$

Note that $\Delta u_\perp$ is positive and the argument of G is negative when $\boldsymbol{u}$ is inside the caustic.

Here G is a characteristic profile function which depends only on the shape of the stellar profile and not on the size of the source. That is, the source size affects the width of the caustic crossing only through the argument $\Delta u_\perp/\rho_*$ of G and the magnification only through the factor $\rho_*^{-1/2}$. For uniform surface brightness, the profile function G reads (Schneider & Weiss 1986b)

$$G_0(\eta) \equiv \frac{2}{\pi} \int_{\max(\eta,-1)}^{1} \left(\frac{1-x^2}{x-\eta}\right)^{1/2} dx\, \Theta(1-\eta) \,, \tag{7}$$

which can be expressed in terms of elliptical integrals. The case of limb-darkened profiles has been discussed by Schneider & Wagoner (1987). Consider an extended source moving over the caustic with proper motion $\mu = \theta_{\rm E}/t_{\rm E}$, at an angle ϕ relative to the caustic. The time required for the radius to cross the caustic is

$$\Delta t = \frac{\theta_*}{\mu \sin \phi} = \rho_* t_{\rm E} \csc \phi \,. \tag{8}$$

Note that the width of the caustic crossing Δt can be measured from the caustic crossing data alone, while the three quantities whose product forms Δt (ρ_*, $t_{\rm E}$, and $\csc\phi$) can only be determined from an analysis of the complete light curve (see § 2.3). The angular separation (normalized to $\theta_{\rm E}$) of the source from the caustic crossing as a function of time is

$$\Delta \boldsymbol{u} = \frac{\boldsymbol{\mu}(t - t_{\rm cc})}{\theta_{\rm E}} \,, \tag{9}$$

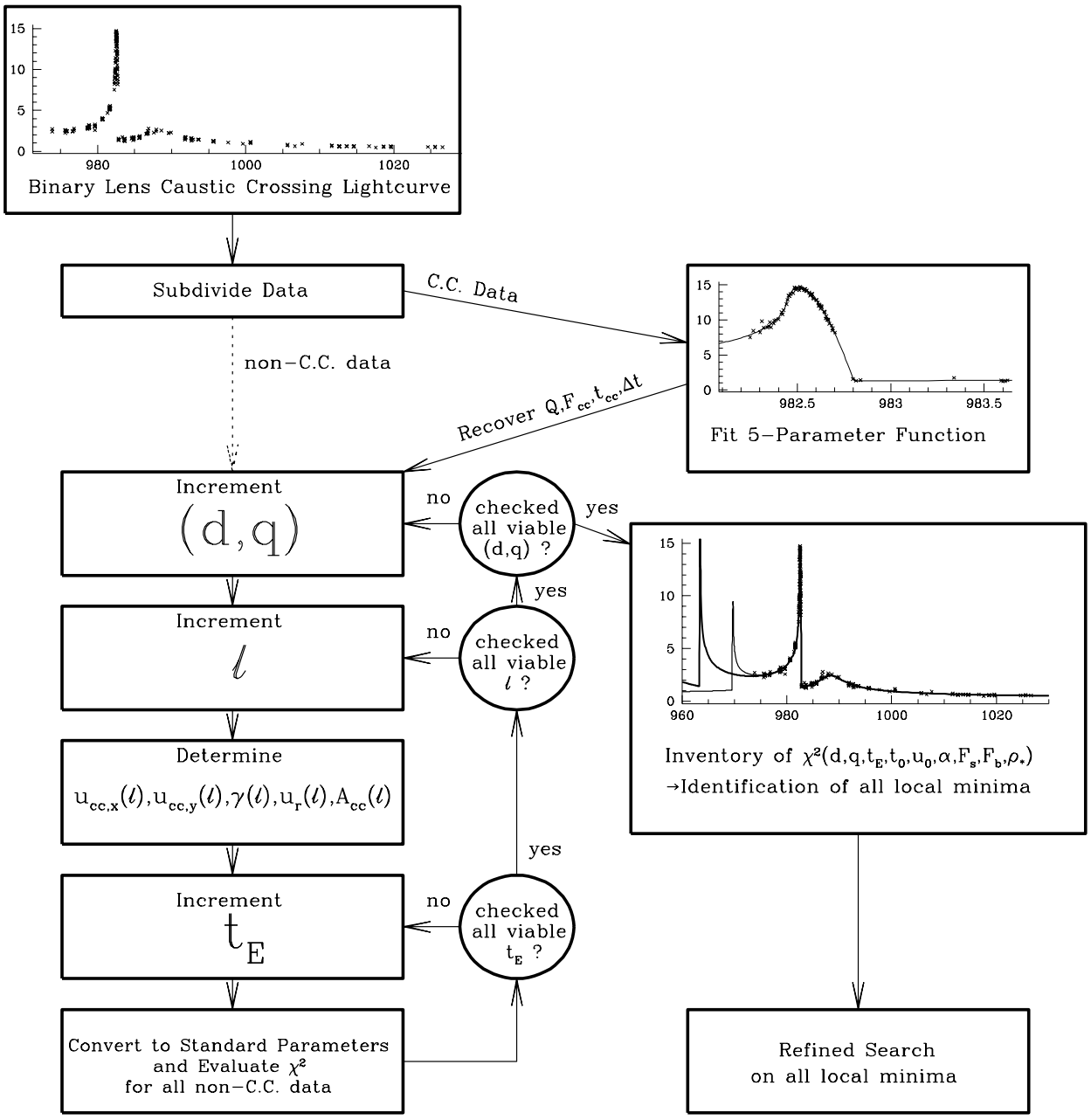

FIG. 1.—Flowchart illustrating the relations among the various steps of the method described in the text

where $\boldsymbol{\mu}$ is the vector proper motion and t_{cc} is the time of the caustic crossing. This implies

$$\Delta u_{\perp} = \frac{\mu(t - t_{cc}) \sin \phi}{\theta_E} = \frac{t - t_{cc}}{t_E} \sin \phi \, . \qquad (10)$$

Hence the magnification as a function of time is given by

$$A(t) = \left(\frac{t_r}{\Delta t}\right)^{1/2} G_0\left(\frac{t - t_{cc}}{\Delta t}\right) + A_{cc} + \omega(t - t_{cc}) \, , \qquad (11)$$

where

$$t_r = u_r t_E \csc \phi \qquad (12)$$

is the characteristic rise time of the caustic crossing and $\omega \equiv \boldsymbol{\mu} \cdot \boldsymbol{Z}/\theta_E$.

If the flux of the source star is F_s and the flux of the blend is F_b, the total flux is given by

$$F(t) = F_s A(t) + F_b = Q^{1/2} G_0\left(\frac{t - t_{cc}}{\Delta t}\right)(\Delta t)^{-1/2} + F_{cc} + \tilde{\omega}(t - t_{cc}) \, , \qquad (13)$$

where $Q = F_s^2 t_r$, $F_{cc} = F_s A_{cc} + F_b$, and $\tilde{\omega} = F_s \omega$. Thus, a caustic crossing can be fitted to a five-parameter function of the form of equation (13), the parameters being Q, t_{cc}, F_{cc}, Δt, and $\tilde{\omega}$. Below, we will use the three parameters Q, t_{cc}, and F_{cc} to constrain the search for fits to the *non–caustic crossing* points on the light curve. The caustic crossing timescale Δt summarizes information about the caustic crossing only and does not affect the remainder of the light curve or its analysis. The slope $\tilde{\omega}$ was introduced

only to allow a more accurate estimate of F_{cc} and will be of no further interest.

It is also possible to parameterize the total flux by

$$F(t) = F_{cc}\left[\left(\frac{t_{r,\rm eff}}{\Delta t}\right)^{1/2} G_0\left(\frac{t - t_{cc}}{\Delta t}\right) + 1 + \omega_{\rm eff}(t - t_{cc})\right], \quad (14)$$

where

$$t_{r,\rm eff} = \left(\frac{F_s}{F_{cc}}\right)^2 t_r = \frac{Q}{F_{cc}^2} \quad (15)$$

is an "effective" rise time and $\omega_{\rm eff} = \omega/F_{cc}$. This parameterization seems to be more appealing, as it replaces the unintuitive parameter Q with $t_{r,\rm eff}$, the effective rise time of the caustic crossing. Unfortunately, in this parameterization, F_{cc} and $t_{r,\rm eff}$ are very highly correlated: we find below for a specific example that the fractional error in $t_{r,\rm eff}$ is about 7 times larger than the fractional error in Q which makes $t_{r,\rm eff}$ substantially less suitable for numerical calculations. We will therefore use the parameterization in equation (13).

Note that in the neighborhood of the end of the caustic crossing

$$G_0(\eta) \rightarrow 2^{1/2}(1 - \eta)\Theta(1 - \eta)\,, \quad (16)$$

and thus an abrupt change of slope occurs at $\eta = 1$. Hence, while for most points on the light curve it is appropriate to use simply the midpoint of the exposure for the time, this approximation breaks down when the time between the midpoint of the exposure and the end of the caustic crossing ($\eta \sim 1$), $\delta t = t - \Delta t - t_{cc}$, is less than half the exposure time, $t_{\rm exp}$, i.e., $|\delta t| < t_{\rm exp}/2$. For this case we integrate equation (16) over the exposure time and find

$$G_0\left(\frac{t - t_{cc}}{\Delta t}\right) \rightarrow 2^{-1/2}\,\frac{(\delta t - t_{\rm exp}/2)^2}{t_{\rm exp}\,\Delta t}\,, \quad \left(|\delta t| < \frac{t_{\rm exp}}{2}\right). \quad (17)$$

2.2. *Relations between Parameterizations*

As shown in the previous subsection, the caustic crossing fit yields the four parameters Q, t_{cc}, Δt, and F_{cc}. Three of the remaining parameters are the same as in the conventional parameterization: the Einstein timescale, t_E, the normalized projected separation between the lenses, d, and the mass ratio, q. The eighth parameter is the baseline flux $F_{\rm base}$ which is often, but not always, well measured. For the final parameter, we adopt the path length ℓ along the caustic curve(s) for the configuration (d, q). This is a logical choice, since we know that the light curve contains a caustic crossing and the trajectory must therefore cross a caustic at some value of ℓ. Below we show how the local properties of the binary lens at ℓ can be used to relate our nonstandard parameters to the more familiar parameters. In our parameterization, the binary lens event is described by the nine parameters (Q, t_{cc}, Δt, F_{cc}, d, q,ℓ, t_E, $F_{\rm base}$) rather than by the nine "standard" parameters (t_E, t_0, u_0, d, q, α, ρ_*, F_s, F_b). In order to use the caustic crossing parameters (Q, t_{cc}, F_{cc}) to constrain the fit to the non–caustic crossing data, we must know the relation between the two parameter sets. This is trivial for t_E, d, and q. Given a binary configuration (d, q), one can determine at each ℓ the following five local properties of the binary lens. The first two are simply the x and y positions of the caustics at ℓ, $u_{cc,x}(\ell)$, and $u_{cc,y}(\ell)$ with respect to the standard coordinate system (i.e., the origin located at the midpoint of the binary and the x-axis coincident with the binary axis). These values can be determined using the algorithm of Witt (1990). The third property is the angle of the caustic with respect to the binary axis at ℓ, $\gamma(\ell)$, which can be found by the same algorithm and by fitting a line to positions offset by $\delta\ell$ from ℓ. The last two properties must be calculated by solving the full binary lens equation. The near-caustic magnification A_{cc} is the sum of the magnifications of the three nondiverging images at the position of the caustic. The caustic divergence, u_r, is defined by equation (2) and can be determined by fitting an inverse square root function to the sum of the magnifications of the two diverging images in the neighborhood of ℓ. Note that all five quantities are functions of (ℓ, d, q). Using these quantities, the relations between the standard parameters and those used in this paper are simple to determine and are given in Table 1. Figure 2 shows the relation between the two sets of parameters graphically for the parameters that do not involve the finite size of the source. Figure 3 shows a detailed view of the finite source crossing the caustic. Note that several of the quantities shown in Figure 3 are not discussed in the text until equation (28) in § 4.1 below.

2.3. *Fitting Non–Caustic Crossing Data: Idealized Case*

We now use our parameterization and the results of the fit to the caustic crossing data to find corresponding binary lens configurations that contain the observed caustic crossing. For illustrative purposes, let us initially assume that both the baseline flux of the event, $F_{\rm base}$, and the three caustic crossing parameters, Q, F_{cc}, and t_{cc}, have been measured with high precision. (Recall that the fourth caustic crossing parameter, Δt, is not used in the analysis of the non–caustic crossing data.) The search for solutions would then be reduced to a four-dimensional space and could be conducted as follows. First, one begins with a binary configuration (d, q), varying the parameter ℓ over the total length of the caustic. At each ℓ in geometry (d, q), one has two equations relating the source and background fluxes: $F_{\rm base} = F_s + F_b$ and $F_{cc} = F_s A_{cc} + F_b$. Thus,

$$F_s = \frac{F_{cc} - F_{\rm base}}{A_{cc} - 1}\,. \quad (18)$$

If $F_s > F_{\rm base}$ (i.e., $A_{cc} < F_{cc}/F_{\rm base}$), then there would be negative background flux. Hence any position ℓ yielding $F_s > F_{\rm base}$ does not correspond to a physical solution, and one can move on to the next value of ℓ. At each physical ℓ,

TABLE 1

RELATIONS BETWEEN PARAMETERIZATIONS

Standard	This Paper
d	d
q	q
t_E	t_E
F_s	$(F_{cc} - F_{\rm base})/(A_{cc} - 1)$
F_b	$F_{\rm base} - F_s$
ρ_*	$(\Delta t/t_E)\sin\phi$
u_0	$-u_{cc,x}\sin\alpha + u_{cc,y}\cos\alpha$
t_0	$t_{cc} - t_E(u_{cc,x}\cos\alpha + u_{cc,y}\sin\alpha)$
α	$\gamma + \phi$, where $\sin\phi = F_s^2\,u_r\,t_E/Q$

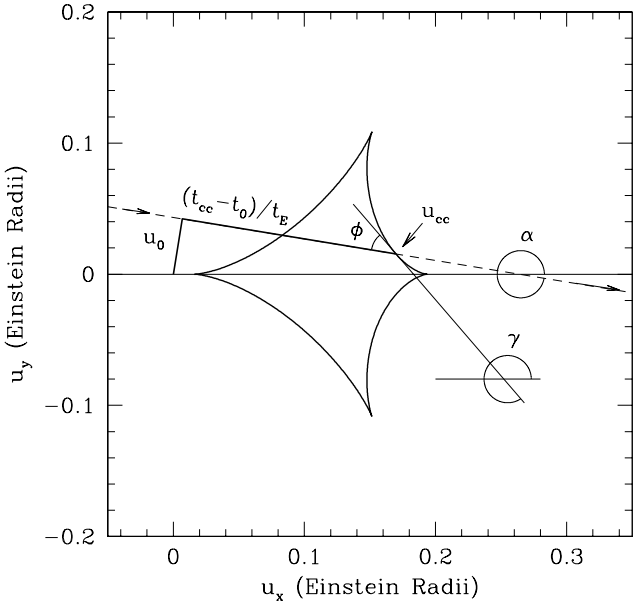

FIG. 2.—Binary lens parameterization. The trajectory of the source (*dashed line*) is inclined by an angle α (351° in this case) relative to the binary axis (M_2 to M_1) (*solid line*). The impact parameter relative to the geometric center of the binary is u_0. The source crosses the caustic (*diamond-shaped curve*) at $\boldsymbol{u}_{cc}$. The difference between this crossing and the point of closest approach at u_0 is shown by a bold line. The tangent to the caustic makes an angle $\gamma = 311°$ with the binary axis. The angle between the source trajectory and the tangent to the caustic is therefore $\phi = \alpha - \gamma = 40°$. The vector position $\boldsymbol{u}_{cc}$ is measured relative to the midpoint of the two masses (0, 0).

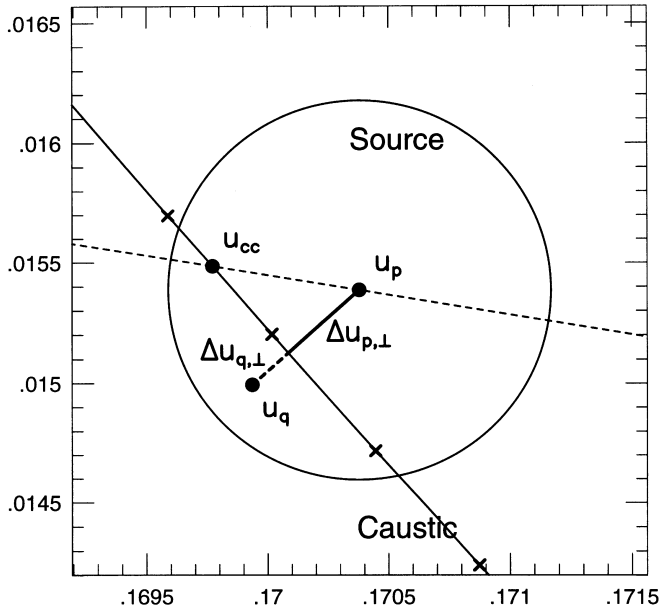

FIG. 3.—Binary lens parameterization (detail). The circle is the source which moves on a trajectory shown by the dashed line. The source crosses the caustic (*solid line*) at position $\boldsymbol{u}_{cc}$, and its current position is $\boldsymbol{u}_p$. The perpendicular distance to the caustic $\Delta u_{p,\perp}$ (*bold line*) is used in eq. (28) and is negative in this case. The position $\boldsymbol{u}_q$ lies along the line perpendicular to the caustic and halfway from the caustic to the edge of the source inside the caustic. The distance $\Delta u_{q,\perp}$ (*bold dashed line*) is also used in eq. (28) and is always positive. If the source lies entirely inside the caustic, then $\boldsymbol{u}_q = \boldsymbol{u}_p$. The bold crosses show the discrete spatial sampling of the caustic ($\sim$800 points) in our calculations. The vector positions $\boldsymbol{u}_{cc}$, $\boldsymbol{u}_p$, and $\boldsymbol{u}_q$ are all measured relative to the midpoint of the two masses (0, 0) which is not shown in this figure but is shown in Fig. 2.

t_E is varied and for each t_E, the angle ϕ at which the source crosses the caustic is determined using equation (12) and the definition $Q \equiv F_s^2 t_r$,

$$\sin \phi = \frac{u_r t_E F_s^2}{Q} . \tag{19}$$

Of course, ϕ must satisfy $\sin \phi \leq 1$, which means that only values of t_E in the range

$$t_E \leq \frac{Q}{u_r F_s^2} \tag{20}$$

need to be searched. Note that ϕ is restricted to lie in the range $0 \leq \phi \leq \pi$ and the orientation of γ is set to enforce the relation in Table 1: $\alpha = \phi + \gamma$. At this point all of the standard parameters needed to evaluate the magnifications at all the times of the observations have been determined. Since F_s and $F_b (= F_{base} - F_s)$ are completely determined for this geometry, these magnifications can be used to predict the flux, $F(t) = F_s A(t) + F_b$, and these predictions can be compared with the data using χ^2. However, before doing the calculation for the entire (non–caustic crossing) light curve, the following checks should be done. From inspection of the light curve, it is often clear which measurements are inside the caustic and which are outside the caustic. One could then evaluate the number of images at the most restrictive of these measurements (i.e., the last measurement before the first crossing and the first measurement after this crossing) and determine whether the model is consistent with these observational constraints. If it is not, no further evaluation need be done and one can continue to the next parameter combination. Thus one can calculate χ^2 for each combination (d, q, t_E, ℓ) and find the best fit (or fits) to the data. The search is over a four-dimensional space, but under restricted circumstances.

2.4. *Non–Caustic Crossing Data: Realistic Case*

In practice, Q, F_{cc}, and F_{base} are not known with infinite precision, and so one must take account of the uncertainties in these parameters. For well-sampled caustic crossings, the time of caustic crossing t_{cc} is measured to much higher precision than is required, so for this purpose we assume that it is known perfectly. The parameter Δt has no effect on the non–caustic crossing data, so uncertainties in this parameter are unimportant. The uncertainties in Q, F_{cc}, and F_{base} introduce two major changes into the above procedure. First, one must consider a *range* of $\sin \phi$ at each parameter combination (d, q, ℓ, t_E) rather than a single value. That is, there is a fifth dimension to the search, albeit over a truncated domain. Second, once a parameter combination (d, q, ℓ, t_E) is chosen, and the range in ϕ to be explored is determined, one must *fit* for the two flux parameters F_s and F_b since these are no longer determined with infinite precision. This appears to add two dimensions to the search, but in fact this is a linear fit and can be computed much more quickly than the other steps required for each combination (d, q, ℓ, t_E, ϕ) (see also Rhie et al. 1999). Thus, the search is effectively increased to 4.5 dimensions. Good constraints on the time of the first caustic crossing restrict the search further as discussed following equation (20).

We now consider the realistic case more closely. Since F_{cc} and F_{base} have uncertainties, so will F_s through equation (18). Then, the uncertainties in F_s and Q will propagate to

the estimate of sin ϕ through equation (19). Since Q and F_{cc} are highly anticorrelated, the error in sin $\phi \propto F_s^2/Q$ will be higher than given by naive error propagation. One then needs to explore a range for sin ϕ (say 2 or 3 σ) rather than the single value derived in the previous section.

Usually, the uncertainty in F_{base} will lie at one of two extremes. Either the baseline is very well known from many observations before or after the event, or it is very poorly known because the event is not yet over. In the latter case, there will of course be baseline measurements made using the telescope from which the event was discovered, but these may not be generally available. Even if they are, they will usually be in a different filter with different seeing conditions and so not directly useful for establishing a baseline for the observations of the caustic crossing (but see § 5.3). In the first case, the error in F_s is simply $(A_{cc} - 1)^{-1}$ times the error in F_{cc}. In the second case, one has only an upper limit, $F_{base} < F_{lim}$. This leads to range of allowed values for F_s,

$$\frac{F_{cc} - F_{lim}}{A_{cc} - 1} \leq F_s \leq \frac{F_{cc}}{A_{cc}}, \quad (21)$$

with the second relation coming from $A_{cc} F_s = F_{cc} - F_b \leq F_{cc}$. This range must then be expanded to allow for errors in F_{cc} before being combined with equation (19) and its associated uncertainties in Q.

Once the four trial parameters (d, q, ℓ, t_E) are chosen, the allowed range in ϕ can be determined. The standard parameters t_0, u_0, and α, which completely specify the trajectory, can be found from the relations in Table 1, and using d, q, and t_E, the magnification can be determined as a function of time. The best fit for the remaining two parameters needed for the noncrossing data, F_s and F_b, can be determined by linear regression. That is, for each noncaustic crossing observation (to be defined more precisely below) at time t_i, one predicts the flux,

$$F_{pred,i} = A^0(t_i) F_s + F_b, \quad (22)$$

and then forms $\chi^2 = \sum_i (F_{pred,i} - F_{obs,i})^2/\sigma_i^2$, where $F_{obs,i}$ is the observed flux and σ_i is the error of the observation at t_i. This does not yet take into account the information about F_s and F_b contained in the caustic crossing data. To include this information, we simply invert equation (19) and note that in the present context, ϕ and t_E should both be regarded as constants. That is, $F_s = [Q \sin \phi/(u_r t_E)]^{1/2}$ and $\sigma_{F_s} = \sigma_Q[\sin \phi/(4Q u_r t_E)]^{1/2}$, where σ_Q is the error in Q taken from the fit to the caustic crossing data. Hence, χ^2 is given by

$$\chi^2 = \sum_i \frac{[A^0(t_i) F_s + F_b - F_{obs,i}]^2}{\sigma_i^2} + 4 \frac{[(Q u_r t_E \csc \phi)^{1/2} F_s - Q]^2}{\sigma_Q^2}, \quad (23)$$

which can be solved for F_s and F_b by standard linear techniques.

Clearly all the points that were not used in the caustic crossing fit can be incorporated into equation (23). In addition, one might also wish to use the points outside the caustic which were included in the caustic crossing fit in order to determine F_{cc} and the slope $\tilde{\omega}$. Since F_{cc} does not directly enter equation (23), this may appear to be permissible. Actually, since F_{cc} is highly correlated with Q, inclusion of these points is not strictly permitted. Nevertheless, we advocate including them (and thus slightly overcounting the information they contain) because the method is being used to find allowed regions of parameter space not to determine the errors of the best fit.

3. A WORKED EXAMPLE: PLANET DATA FOR MACHO 98-SMC-01

To illustrate how the method works, we apply it to the PLANET data for MACHO 98-SMC-1. These data differ from those analyzed by Albrow et al. (1999a) in two ways: the South African Astronomical Observatory (SAAO) data have been rereduced using a better template, and a few late times points that became available only later have been added. In addition, we now report the Heliocentric Julian Date (HJD) rather than Julian Date (JD) and uniformly report the midpoints of the exposures, rather than their beginnings, as was previously done for some of the observatories. We choose this example because it has a well-covered caustic and the data are publicly available.[8]

3.1. *Choosing the Data Set for the Caustic Crossing Fit*

The first step is to fit the caustic crossing, and to do this we must choose which data points should be used for the fit. The entire data set is shown in Figure 4. Data within 1.5 days of the caustic crossing (HJD 2,450,000.0 = 982.6 ± 1.5) are shown as individual points while the rest are shown as daily averages. Figure 5 shows the immediate neighborhood of the crossing in more detail.

What should be the first point included in the caustic crossing fit? When the source is too close to the caustic, it cannot be approximated as a point source and so cannot be included in the non–caustic crossing fit. Hence, these observations should be included in the caustic crossing fit. This condition can be understood precisely because, from equation (7), $G_0(\eta)$ can be expanded in the limit $\eta \ll -1$,

$$G_0(\eta) = (-\eta)^{-1/2}(1 + \tfrac{3}{32}\eta^{-2} + \ldots), \quad (\eta < -1). \quad (24)$$

Hence, for typical daily averaged photometry errors of $\lesssim 1\%$, this cutoff should be about three source radius crossing times before the time of the caustic crossing, i.e., at $t = t_{cc} - 3\Delta t$, where the fractional effect of the finite source is $(3/32)\eta^{-2} \sim 1\%$. For well-sampled crossings, one can estimate Δt and t_{cc} by eye and use these estimates to determine which data should be included. As we show below, for this data set $\Delta t \sim 0.18$ days and $t_{cc} \sim 982.62$ days, so data after $t \sim 982.08$ should be included. Another important consideration is that the magnifications too far before the crossing will not be well approximated by equation (7), primarily because the two divergent images will not be well approximated by equation (2). If the time that the source spends inside the caustic is not long compared with Δt, then this condition cannot be satisfied simultaneously with the previous one and the method breaks down. This might happen either because the caustic is very small (e.g., a planetary caustic) or because the crossing is close to a cusp. Other methods must then be used (e.g., Gaudi & Gould 1997; Albrow et al. 1999b). From Figure 4, however, the ratio of these two times is at least 50 in the present case, so this is not a major concern.

What should be the last point included? Sufficient data after the crossing are required to establish the slope $\tilde{\omega}$ well enough to extrapolate back "under" the high magnification peak ($t_{cc} \pm \Delta t$) and so establish the value of F_{cc}. In the

[8] http://www.astro.rug.nl/~planet.

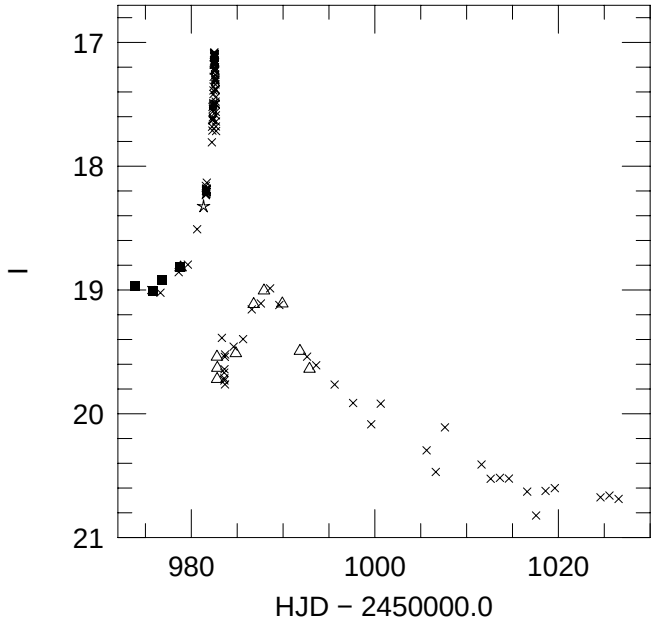

FIG. 4.—PLANET *I*-band data for the binary microlensing event MACHO 98-SMC-1 from four observatories, SAAO 1 m (*crosses*), Yale-CTIO 1 m (*triangles*), CTIO 0.9 m (*squares*), and Canopus 1 m (Tasmania) (*star*). Individual points are shown for the interval $t = 982.6 \pm 1.5$. The remaining points are daily averages at the individual observatories.

present case, the three Yale points near 982.8 days are too close to the end of the caustic crossing for this purpose. The next set of points are the SAAO data near 983.6 days. Fortunately, the cusp-approach "bump" centered near 988 days is sufficiently far from these SAAO observations that they can be used. In general one might not be so lucky, and the choice of a final cutoff for data to be included in the caustic crossing fit should be made carefully.

Altogether, there are 74 data points in the caustic crossing region, 71 from SAAO and three from Yale. Since these data come from two different telescopes, they could in principle have different values of F_s and F_b. Since the caustic crossing itself does not possess sufficient information to determine the relative values of F_s and F_b, either external information must be applied or data from one of the observatories must be ignored. The latter choice would be tolerable in the present case because there are only three Yale points and, as we will show, these reduce the error bars of the caustic crossing parameters by only about 20%. In general, however, fitting the crossing may depend critically on data from several observatories. Even in the present case, using all the data would be preferable. To do so, we first make an initial educated guess as to the relative values, namely, that F_s and F_b are both the same for the two observatories. (In the present case, F_s is known a priori to be the same because the two observatories use similar filters and the photometric measurements are made relative to the same reference stars. However, the two F_b could be different because the reductions are not carried out with the same template and so different amounts of background light could enter the photometric apertures.) We then search for solutions using the non–caustic crossing data. We find that all viable solutions have $F_b^{\rm SAAO} \simeq F_b^{\rm Yale} + 0.039F_{20}$, where F_{20} is the flux from an $I = 20$ star. The scatter ($0.04F_{20}$) in these determinations is smaller than the $0.08F_{20}$ combined error for the three Yale measurements, so we simply employ the offset without incorporating an additional uncertainty.

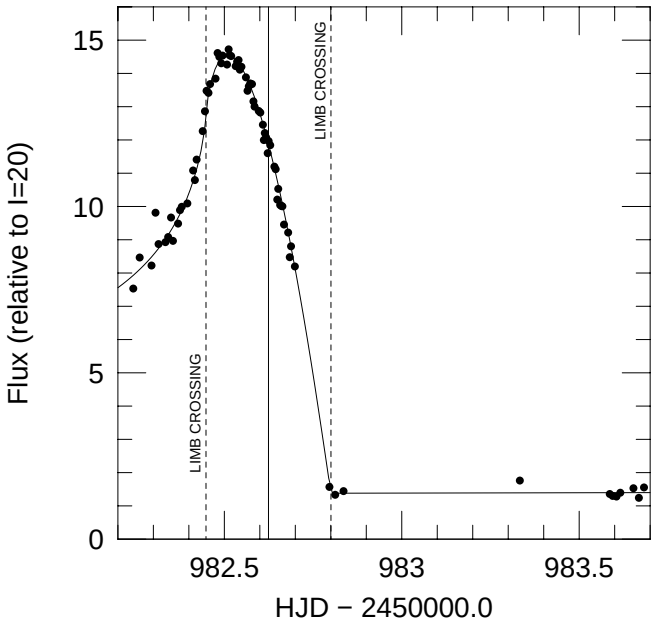

FIG. 5.—PLANET *I*-band data for the caustic crossing region of the binary microlensing event MACHO 98-SMC-1. Fluxes are shown in units of F_{20}, the flux from an $I = 20$ star. All points are from the SAAO 1 m except the three near $t = 982.8$ which are from the Yale-CTIO 1 m. These have been increased by $0.039F_{20}$ as described in the text. The solid vertical line at $t_{\rm cc} = 982.624$ is the fit value for the time that the center of the star crossed the caustic. The two dashed vertical lines at $t = t_{\rm cc} \pm \Delta t$, where $\Delta t = 0.176$, are the fit values for the time when the limbs crossed the caustic.

3.2. *Caustic Crossing Parameters*

We find fit parameters,

$$Q = (15.73 \pm 0.35)F_{20}^2 \text{ days},$$
$$t_{\rm cc} = (982.62439 \pm 0.00087) \text{ days},$$
$$\Delta t = (0.1760 \pm 0.0015) \text{ days}, \quad (25)$$
$$F_{\rm cc} = (1.378 \pm 0.096)F_{20}, \quad \tilde{\omega} = (0.02 \pm 0.10)F_{20} \text{ day}^{-1}, \quad (26)$$

with a matrix of coefficients of local correlation

$$\begin{pmatrix} 1.00 & 0.45 & 0.64 & -0.97 & 0.91 \\ 0.45 & 1.00 & 0.76 & -0.39 & 0.32 \\ 0.64 & 0.76 & 1.00 & -0.57 & 0.52 \\ -0.97 & -0.39 & -0.57 & 1.00 & -0.93 \\ 0.91 & 0.32 & 0.52 & -0.93 & 1.00 \end{pmatrix}, \quad (27)$$

where the order of the rows and columns corresponds to the order of the parameters in equations (25) and (26). The effective rise time of the caustic crossing is $t_{r,\rm eff} = (8.28 \pm 1.34)$ days. Note that the midpoint of the first Yale data point occurs 4 minutes before the best-fit time for the end of the crossing. Since the exposure time was $t_{\rm exp} = 20$ minutes, we use equation (17) for this point.

For completeness, we note that if we ignore the Yale data, we obtain $Q = (15.73 \pm 0.41)F_{20}^2$ days, $t_{\rm cc} = (982.62444 \pm 0.00096)$ days, $\Delta t = (0.1761 \pm 0.0017)$ days, $F_{\rm cc} = (1.379 \pm 0.115)F_{20}$, and $\tilde{\omega} = (0.02 \pm 0.12)F_{20}$ day^{-1}.

Figure 5 shows the best-fit curve to the caustic crossing. It has $\chi^2 = 113$ for 69 dof. We therefore estimate that the formal DoPHOT errors should be multiplied by $(113/69)^{1/2} = 1.28$, and we use these higher errors in all subsequent work. This ratio between formal errors and true uncertainties is typical of DoPHOT-reduced PLANET data (Albrow et al. 1998).

We note in passing that the end of the caustic crossing occurred at $t = t_{cc} + \Delta t = 982.8004 \pm 0.0028$. This may be compared with the values obtained by EROS from their detailed observations of the end of the caustic crossing, 982.8037 ± 0.0012 and 982.8047 ± 0.0021 for their blue and red filters, respectively (Afonso et al. 1998), where we have converted the EROS numbers from JD to HJD and corrected a 0.005 day error in the global zero point in the EROS times (E. Aubourg 1999, private communication).

In this paper we do not generally consider limb darkening. However, as we show in Appendix B, it is straightforward to incorporate a limb-darkening parameter into the analysis of the caustic crossing. In this case we find in place of equations (25) and (26) the values $Q = (15.55 \pm 0.35)F_{20}^2$ days, $t_{cc} = (982.62388 \pm 0.00098)$ days, $\Delta t = (0.1765 \pm 0.0015)$ days, $F_{cc} = (1.375 \pm 0.097)F_{20}$, and $\tilde{\omega} = (0.02 \pm 0.10)F_{20}$ day^{-1}. The difference between these parameters and the non–limb-darkened ones quoted above are not significant.

3.3. *Grid of Lens Parameters*

In principle, the lens could have any geometry (d, q), with $0 < d < \infty$ and $0 < q \leq 1$. We must therefore choose a grid of geometries that adequately samples this space. We initially choose arrays of values $q = 0.005, 0.01, 0.03, 0.05, 0.1, 0.3, 0.5, 0.75, 1.0$ and $d = 0.3, 0.4, 0.5, 0.6, 0.7, 0.8, 0.9, 1.0, 1.2, 1.4, 1.7, 2.0, 2.5, 3.0, 3.5, 4.0, 4.5$. We will see in § 4 that this is adequate. For the Einstein crossing times, we choose a range 20 days $\leq t_E \leq$ 200 days. Our observations display significant structure for at least 25 days beginning at about the minimum of the caustic region, so it is very unlikely that the event could be shorter than 20 days. In fact the event could be longer than 200 days if it were heavily blended, in which case only the inner, highly magnified portions of the Einstein ring would give rise to significant structure. In this case, we would find that for each geometry near the geometry characterizing the actual event, the lowest χ^2 fit would have durations at or near our upper limit of $t_E = 200$ days.

For each geometry we first create a very densely sampled representation of the caustic using the algorithm of Witt (1990), which is unevenly sampled with much wider spacing near the cusps than between them. We then resample each of the 1–3 closed caustic curves with about 800 roughly equally spaced points, ℓ_i. At each point we evaluate $A_{cc}(\ell_i)$ directly on the caustic and $u_r(\ell_i)$ by sampling the magnification at distances $\Delta u_\perp = 0.0001, 0.00004, 0.00002$, and 0.00001 and applying equation (2). This procedure of course fails in the neighborhood of the cusps, but since the largest trial value of $\Delta u_\perp$ is more than 10 times smaller than the source, any caustic position where the procedure fails is not a viable candidate for a fold caustic crossing in any case.

The event was not yet at baseline at the last data point. We therefore can estimate only an upper limit $F_{lim} > F_{base}$ for the baseline flux. We choose $F_{lim} = 0.55F_{20}$ based on the upper limit from the last three measurements (see Fig. 4).

We find that stepping through the ~ 800 caustic points ℓ_i yields a $\chi^2_{min}(\ell_i)$ as a function of position ℓ_i that is sufficiently well sampled to obtain at least one point with χ^2_{min} that is within 1 or 2 of the true local minimum.

At each position we sample the range of timescales t_E in increments of 5%. This choice is dictated by the character of the cusp-approach structure seen in Figure 4 with a peak near $t = 988$ days. The FWHM and the time from the caustic crossing are about equal, approximately 6 days. The 14 daily averaged measurement errors are typically $\sigma \sim 4\%$. Hence a deviation of the trial t_E from the true value by $\delta \sim 2.5\%$ would lead to a change in χ^2 of $\sim 14(\sigma/2\delta)^2 \sim 1$. For each t_E, we explore the range of $\sin\phi$ described by equations (19) and (21) and augmented by the 3 σ errors for Q (eq. [25]), stepping in 5% increments. Other choices of increment size could be made. Empirically, we find that with our adopted choice of 5% timescale increments, the search can miss a local minimum in χ^2 by $\Delta\chi^2 \sim 10$. This means that all local minima lying within $\Delta\chi^2 \sim 15$ of the global minimum must be checked (see § 4).

For each geometry (d, q) we record the lowest value of χ^2 and examine the resulting map. We find three very broad areas of (d, q) space with very similar values of $\chi^2 \sim 130$–135. These are roughly described by $(0.4 \lesssim d \lesssim 0.7) \times (0.3 \lesssim q \lesssim 1)$, $(2.5 \lesssim d \lesssim 3.5) \times (0.1 \lesssim q \lesssim 1)$, and $(0.6 \lesssim d \lesssim 0.7) \times (0.05 \lesssim q \lesssim 0.1)$. That is, we appear to have found an extremely broad class of solutions rather than a single unique minimum or even a few well-defined isolated minima.

For several individual (d, q) pairs, we also examine the minimum χ^2 *as a function of position* ℓ around the caustics. Typically, we find two distinct minima with comparable χ^2, one with α close to 0 (or 2π) and the other with $\alpha \sim \pi$. These describe second caustic crossings on opposite sides of the caustic region. We therefore conduct two automated searches at each (d, q), one with $\pi/2 \leq \alpha < 3\pi/2$ and the other in the complementary region. We remark on the relation between these two solutions at the end of § 4.

4. WORKED EXAMPLE II: REFINED SEARCH FOR MINIMA

In order to investigate this preliminary result further, we search for local minima near the solutions with $\chi^2 \lesssim 145$, found at each (d, q) encompassing a slightly larger region than the broad apparent plateau discussed at the end of § 3.3. We adopt this somewhat looser criterion because, as we discussed above, the initial systematic search could miss the true minimum by $\Delta\chi^2 \sim 10$.

4.1. *Basic Approach*

Although the standard procedure in such a search would be to allow all parameters to vary simultaneously, we specifically *do not* follow this usual approach. Instead, we hold d and q fixed and allow only the remaining parameters to vary. This will permit a test of the hypothesis that there is a set of very broad minima in (d, q) space. If the χ^2 minimum at each of these points is essentially the same, then d and q are indeed highly degenerate. On the other hand, if the minimum χ^2 is found to differ substantially for different fixed (d, q), then it would be worthwhile to allow these parameters to vary simultaneously with the others.

For each set of trial parameters, we proceed as follows. For each observation (not binned by day as in the preliminary search), we evaluate the magnification by one of two methods, both semianalytic. If the source lies entirely

outside of the caustics or if its center lies at least 3.5 source radii from a caustic, we simply use the magnification at the source center. Otherwise, we use an approximation for the magnification that is similar in spirit to the approximation used to fit the caustic crossing that we introduced in § 2.1:

$$A(\boldsymbol{u}_p) = A_3^0(\boldsymbol{u}_p) + A_2^0(\boldsymbol{u}_q)\left(\frac{\Delta u_{q,\perp}}{\rho_*}\right)^{1/2} G_0\left(-\frac{\Delta u_{p,\perp}}{\rho_*}\right), \quad (28)$$

where $\boldsymbol{u}_p$ is the position in the Einstein ring of the center of the source, $\boldsymbol{u}_q$ is another position in the Einstein ring to be described below, $\Delta u_{p,\perp}$ and $\Delta u_{q,\perp}$ are, respectively, the perpendicular distances from $\boldsymbol{u}_p$ and $\boldsymbol{u}_q$ to the nearest caustic, $A_3^0(\boldsymbol{u}_p)$ is the magnification of the three nondivergent images at the position $\boldsymbol{u}_p$, $A_2^0(\boldsymbol{u}_q)$ is the magnification of the two divergent images at the position $\boldsymbol{u}_q$, and ρ_* is the source size in units of the Einstein ring. If $\Delta u_{p,\perp} > \rho_*$, then we assign $\boldsymbol{u}_q = \boldsymbol{u}_p$. Otherwise, we take $\boldsymbol{u}_q$ to lie along the perpendicular to the caustic through $\boldsymbol{u}_p$ and halfway from the caustic to the limb of the star that is inside the caustic. The argument of G_0 is negative if the center of the source lies inside the caustic and positive if it lies outside.

Note that for the second term in equation (28) to be well defined, the argument of A_2^0 *must* be a point inside the caustic. This is the reason for choosing a $\boldsymbol{u}_q$ different from $\boldsymbol{u}_p$. If the approximation given by equation (2) (and so eq. [6]) were exact, then equation (28) would be valid with *any* choice of $\boldsymbol{u}_q$ inside the caustic. Since equation (2) is not exact, we choose $\boldsymbol{u}_q$ at the middle of the part of the source inside the caustic in order to minimize the error.

As we discussed in § 2, this approximation should work well whenever the source is small compared with the distance between caustic crossings and with the distance from a caustic crossing to the nearest cusp. It will not work for small (e.g., planetary) caustics or cusp crossings.

The advantage of this approximation is that it allows one to evaluate the magnifications for the several hundred points on the light curve in less than 1 s, compared with the several minutes required for a numerical integration over the source. This advantage will come into play when we discuss our minimization technique below.

Once the magnifications have been calculated we fit for the flux parameters. Recall that for a single observatory there are two parameters, F_s and F_b. In this example, there are four observatories, Canopus 1 m, CTIO (Cerro Tololo Inter-American Observatory) 0.9 m, SAAO 1 m, and Yale 1 m, which seem to imply eight flux parameters. However, since all four observatories use very similar *I*-band filters and reduce the images relative to a common set of local standards, we take F_s to be the same for all four. In addition, we take the F_b for Canopus to be the same as SAAO because there is only one data point (and so no room for another parameter) and because it is a high magnification point, so differences in F_b are unlikely to be important. The linear fit to the remaining four parameters requires very little time to compute (see also Rhie et al. 1999).

Since d and q are held fixed and F_b and F_s are determined by linear regression, there remain five parameters to fit. These are normally taken to be t_0, u_0, t_E, α, and ρ_*. However, as discussed in § 2, the time of the caustic crossing, t_{cc}, and the caustic crossing time, Δt, are much better determined than either t_0 or ρ_*; we therefore use the former in place of the latter. While both t_{cc} and Δt are allowed to vary, both tend to move over very small ranges that are consistent with the results from the caustic crossing fit in § 3.2. Nevertheless, despite the fact that two parameters are held fixed and two others are relatively well constrained, we find that it is not easy to locate local minima. We suspect that the χ^2 function is quite complicated. Moreover, in order to properly explore parameter space, it is necessary to repeat the minimization procedure for several dozen different (d, q) pairs, and this will be multiplied severalfold in the next section.

We therefore take advantage of the efficient method of magnification calculation summarized in equation (28), which makes possible a rather cumbersome, but fairly robust, method of minimization. For each parameter a_i we establish a grid size, δ_i, and for every new set of trial parameters evaluate χ^2 at the 51 positions $(a_i + \epsilon_i \delta_i)$, where $\epsilon_i = -1, 0, +1$ and $\sum_i |\epsilon_i| \leq 2$. At each step, the operator is allowed one of three options: move to the lowest value of the 51 positions, move to (or toward by a specified fraction) the predicted minimum of the best-fit quadratic to the χ^2 surface, or adjust the grid size. In practice, the procedure is semiautomated so as not to bother the operator while the routine is making adequate progress.

We find that even with this extensive probing of the neighborhood of the trial solution, the path to lower χ^2 is not always apparent. For example, sometimes none of the 50 probes of parameter space has a lower χ^2 than the central position, even if the grid size is decreased by a factor 2 or 4. We then move toward the best estimate of the minimum that is derived from the quadratic fit and find that this also has higher χ^2. However, starting from this new central position, some of the 50 new probes have substantially lower χ^2. Moreover, for the next iterations the path downward is clear and χ^2 may drop by 2–10 over these next few steps. We do not understand the nature of these "hang-ups." In principle, it is possible they are due to genuine local minima, but we suspect that the χ^2 surface is just extremely complicated and that the paths toward lower values are narrow and not well probed even by our 50 trial points. Although skepticism is warranted, we believe that the true local minimum is eventually reached, for two reasons. First, as we show in the next section, we find many different solutions with almost exactly the same χ^2. It would be a remarkable coincidence if the search process always stalled at the same value of χ^2. Second, if the first attempt does not approach this minimum, we try several other "paths" and we find that there are no significant improvements after the second or third try. Nevertheless, this experience counsels us to be cautious about the interpretation of apparent minima.

4.2. *Solutions*

We search for refined solutions (see § 4.1) near each of the rough solutions found in § 3 considering only those within 2.5 σ (i.e., $\Delta\chi^2 < 6.25$) of the minimum value found for the entire grid. We find 41 such solutions including *all* combinations of $d = (0.4, 0.5, 0.6, 2.5, 3.0, 3.5)$ and $q = (0.3, 0.5, 0.75, 1.0)$, plus additional solutions at $(d, q) = (0.6, 0.1)$, $(0.7, 0.05)$, $(0.7, 0.1)$, and $(0.7, 0.3)$. This appears to be only 28 solutions, but for many (d, q) pairs we find two distinct solutions, one at $\alpha \sim 0$ (or 2π) and the other at $\alpha \sim \pi$.

Table 2 shows the 41 solutions. The first seven columns are the parameters d, q, α, u_0, t_E, t_{cc}, and Δt. The next two are the x and y components of $\boldsymbol{u}_{cc}$, the point of the caustic crossing. These are shown in order to allow easy transform-

TABLE 2

SOLUTIONS FOR MACHO 98-SMC-1

d	q	α (deg)	u_0	t_E (days)	t_{cc} (days)	Δt (days)	$u_{cc,x}$	$u_{cc,y}$	F_s (F_{20})	F_b (F_{20})	I_{base}	t_* (hr)	$\Delta\chi^2$
0.4	0.30	176.288515	0.000731	227.07191	982.62308	0.17763	0.0505407	−0.0040111	0.065	0.248	21.262	1.26	1.13
0.4	0.50	176.160188	0.005100	191.37500	982.62267	0.17622	0.0066413	−0.0055568	0.077	0.244	21.232	1.50	0.86
0.4	0.75	176.356646	0.008389	181.21332	982.62296	0.17820	−0.0291313	−0.0065511	0.082	0.245	21.214	1.73	1.88
0.5	0.30	177.055544	0.004082	146.34175	982.62301	0.17718	0.0409234	−0.0061919	0.106	0.230	21.183	1.32	0.00
0.5	0.50	176.464213	0.009445	125.60321	982.62276	0.17901	−0.0108846	−0.0087901	0.123	0.228	21.137	1.60	1.66
0.5	0.75	175.932138	0.014927	115.19602	982.62303	0.17795	−0.0508238	−0.0113502	0.133	0.223	21.120	1.87	1.88
0.5	1.00	174.979970	0.019726	113.45692	982.62307	0.17799	−0.0780739	−0.0129435	0.134	0.227	21.106	2.04	1.52
0.6	0.10	178.672061	0.000108	174.22601	982.62284	0.17820	0.1367621	−0.0032782	0.094	0.228	21.231	0.91	4.28
0.6	0.30	177.105498	0.008148	102.13599	982.62299	0.17759	0.0233205	−0.0093372	0.160	0.205	21.093	1.40	1.48
0.6	0.50	176.676879	0.015201	88.81584	982.62295	0.17869	−0.0341377	−0.0132440	0.182	0.201	21.041	1.73	3.77
0.6	0.75	174.951784	0.024528	81.29927	982.62309	0.17737	−0.0764390	−0.0178711	0.195	0.198	21.014	2.00	3.72
0.7	0.05	181.353672	0.001800	168.88968	982.62213	0.17669	0.1924431	0.0027466	0.103	0.212	21.253	0.70	1.43
0.7	0.10	177.965535	0.001337	112.28410	982.62268	0.17768	0.1262083	−0.0058217	0.158	0.181	21.175	0.96	1.66
0.7	0.30	177.363661	0.013466	75.87443	982.62296	0.17765	−0.0015930	−0.0134074	0.230	0.167	21.003	1.54	4.94
2.5	0.75	172.537435	0.159362	93.67091	982.62312	0.17887	−1.0713230	−0.0203930	0.217	0.184	20.989	2.53	4.34
3.0	0.30	174.495270	0.134250	139.86790	982.62316	0.17841	−1.2861236	−0.0109252	0.194	0.195	21.024	2.16	3.37
3.0	0.50	173.954132	0.150827	137.26909	982.62300	0.17864	−1.3195142	−0.0119164	0.167	0.209	21.059	2.26	2.71
3.0	0.75	173.181036	0.172416	140.58842	982.62291	0.17653	−1.3476796	−0.0124908	0.146	0.217	21.101	2.36	1.33
3.0	1.00	181.836555	0.034642	121.39940	982.62266	0.17846	1.2346168	0.0049278	0.137	0.226	21.101	0.95	6.20
3.5	0.30	174.867363	0.147047	200.56957	982.62313	0.17756	−1.5634588	−0.0072065	0.137	0.223	21.109	2.06	2.02
3.5	0.50	174.495276	0.160684	192.99286	982.62291	0.17823	−1.5921809	−0.0079863	0.120	0.228	21.144	2.16	1.41
3.5	0.75	172.607000	0.216670	193.56250	982.62314	0.17792	−1.6162541	−0.0087720	0.105	0.230	21.184	2.21	0.75
0.4	0.50	354.289660	0.018770	193.86155	982.62322	0.17737	0.1040713	0.0084569	0.075	0.252	21.212	2.24	1.20
0.4	0.75	354.725312	0.015056	179.12400	982.62309	0.17797	0.0754032	0.0081585	0.082	0.248	21.203	2.02	0.99
0.4	1.00	355.570187	0.011595	175.99900	982.62308	0.17786	0.0528234	0.0075373	0.084	0.245	21.209	1.88	1.09
0.5	0.30	350.681164	0.042772	144.28852	982.62342	0.17751	0.1697713	0.0154856	0.102	0.246	21.146	2.73	0.58
0.5	0.50	352.343467	0.033849	120.86487	982.62328	0.17743	0.1354380	0.0159459	0.123	0.235	21.115	2.46	0.30
0.5	0.75	354.063276	0.024936	114.79706	982.62322	0.17762	0.1035920	0.0142983	0.131	0.232	21.101	2.21	0.72
0.6	0.10	344.066614	0.088806	186.56109	982.62383	0.17844	0.2614569	0.0177111	0.081	0.260	21.170	3.42	5.60
0.6	0.30	348.673257	0.066313	98.75121	982.62358	0.17775	0.2065000	0.0262669	0.153	0.229	21.043	2.99	2.44
0.6	0.50	351.899947	0.048680	85.34718	982.62339	0.17769	0.1691894	0.0250912	0.180	0.216	21.006	2.70	3.35
0.6	0.75	354.149805	0.035537	81.87650	982.62332	0.17784	0.1347917	0.0219126	0.190	0.209	20.995	2.43	4.66
0.6	1.00	355.336898	0.027670	82.63775	982.62320	0.17803	0.1081063	0.0189440	0.191	0.209	20.996	2.22	5.96
2.5	0.30	350.576688	0.206486	172.21305	982.62340	0.17826	1.1802049	0.0134359	0.092	0.237	21.208	2.89	1.69
2.5	0.50	350.192530	0.212932	127.43660	982.62339	0.17843	1.1479990	0.0176425	0.132	0.220	21.136	2.77	1.15
2.5	0.75	352.030376	0.174139	108.11969	982.62324	0.17869	1.1183374	0.0192701	0.167	0.206	21.070	2.72	2.58
2.5	1.00	352.025442	0.171848	99.40422	982.62320	0.17884	1.0952210	0.0200988	0.192	0.197	21.026	2.61	3.24
3.5	0.30	2.555170	0.061240	178.69460	982.62272	0.17901	−1.4704734	−0.0043200	0.142	0.225	21.087	1.19	4.75
3.5	0.50	2.121960	0.051164	173.31940	982.62273	0.17819	−1.4928449	−0.0041142	0.123	0.235	21.116	1.12	5.20
3.5	0.75	2.082320	0.051315	177.21380	982.62244	0.17791	−1.5188600	−0.0038759	0.107	0.240	21.148	1.07	4.07
3.5	1.00	2.418032	0.061305	184.21347	982.62256	0.17787	−1.5414734	−0.0037336	0.096	0.243	21.177	1.04	2.89

ation into other parameterizations of the geometry. The tenth and eleventh columns show F_s and F_b (from SAAO), and the twelfth column is their sum, $F_{base} = F_s + F_b$, expressed as a magnitude, $I_{base} = 20 - 2.5 \log F_{base}$. The thirteenth column is $t_* \equiv \Delta t \sin \phi$. Recall that the proper motion is given by $\mu = \theta_*/t_*$. Finally, the last column is $\Delta\chi^2$, defined by

$$\Delta\chi^2 \equiv \frac{\chi^2 - \chi^2_{min}}{\chi^2_{min}/\mathrm{dof}}\,, \tag{29}$$

where $\chi^2_{min} = 467.95$ is the minimum value of χ^2 found in our search at $(d, q) = (0.5,0.3)$ and dof $= 212 - 11 = 201$ is the number of data points minus the number of parameters.

(Note that the fluxes are calibrated to the Cousins system based on comparison to OGLE stars. See Albrow et al. 1999a.) We reiterate that the solutions shown in Table 2 assume a uniform source, i.e., no limb darkening.

The basic result illustrated by Table 2 is that a broad range of parameters is permitted by the data. Two very broad regions in (d, q) space, one with $d < 1$ and the other with $d > 1$ are permitted. Indeed, there is a rough symmetry $d \leftrightarrow d^{-1}$ which was theoretically predicted by Dominik (1999b). There is also a third, smaller region centered at $(d, q) \sim (0.7, 0.1)$. As expected, t_{cc} and Δt lie in an extremely narrow range since they are primarily determined by the caustic structure and not the global parameters. The full solutions for both t_{cc} and Δt deviate by about 0.0015 days ($\sim$2 minutes) from the caustic crossing solution given in equation (25). This shows that the global parameters do have some influence on the determination of the caustic crossing parameters, although it is quite small. More striking is the large variation in permitted Einstein crossing timescales t_E, from 81 to 227 days. Also of note is the wide variation in allowed values of t_*, from 0.70 to 3.42 hours.

Of course, the fact that there are 41 solutions rather than some other number is a result of our specific choice of grid. Since Table 2 shows very little structure in $\Delta\chi^2$ over broad

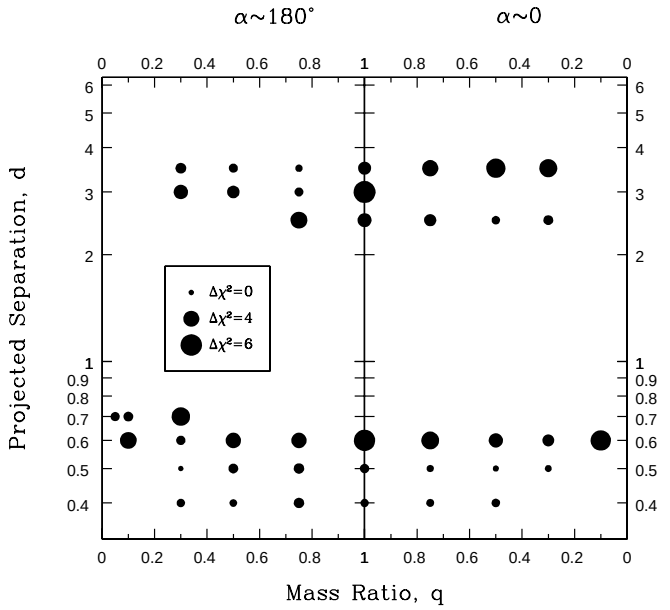

FIG. 6.—Binary lens solutions as listed in Table 2 as a function of mass ratio q and normalized projected separation d. Larger dots indicate higher $\Delta\chi^2$. To the left are the solutions with $\alpha \sim 180°$ which are described in the top half of Table 2, and to the right are the solutions with $\alpha \sim 0$ which are described in the bottom half of Table 2. The points with $q = 1$ can equally well be ascribed to either angle.

ranges of (d, q) space, we expect that a finer grid would not yield any additional information. Figure 6 shows the behavior of χ^2 over the regions of (d, q) space for which $\Delta\chi^2 \leq 6.25$, i.e., the regions covered by Table 2. Note that there are two broad contiguous regions of allowed solutions. Each includes areas with $\alpha \sim 0$ and $\alpha \sim 180°$. For $q = 1$, the caustic is symmetric, so these two angles refer to the same solution, as indicated in the figure.

How different are the light curves associated with these various fits? Figures 7–9 show four representative examples, two from the $d > 1$ region and two with $d < 1$. Each figure contains a curve for $(d, q) = (0.5, 0.3)$, the nominal "best fit," and also one other, for $(d, q) = (3.5, 0.75)$, (0.7, 0.05), and (0.6, 0.75), respectively. All four solutions have $\alpha \sim \pi$ (see Table 2). In Figure 7 the caustic crossing region is shown separately. This is not done for the other two figures because the caustic crossing regions look identical for all four solutions. All light curves are normalized to the SAAO data by subtracting $\Delta F = F_{b,i} - F_{b,\mathrm{SAAO}}$, i.e., the difference in the fit values for the backgrounds as measured at the two observatories. In each case, the two light curves are barely distinguishable over the time period covered by the data. This shows that a wide variety of geometries can produce essentially identical light curves if one is restricted to data covering the "second half" of the event. On the other hand, in the regions that are not covered, the light curves can differ dramatically.

An important corollary to this observation is that, by time reversal, it is impossible to accurately predict the time of the second caustic crossing even from extremely good data covering the first. The second caustic crossing can only be predicted by frequent monitoring of the event and looking for the inverse square root behavior as the second caustic approaches. Indeed, this is how the second caustic crossing of MACHO 98-SMC-1 was predicted by PLANET; the predictions of MACHO close to the caustic crossing were made in this way as well.

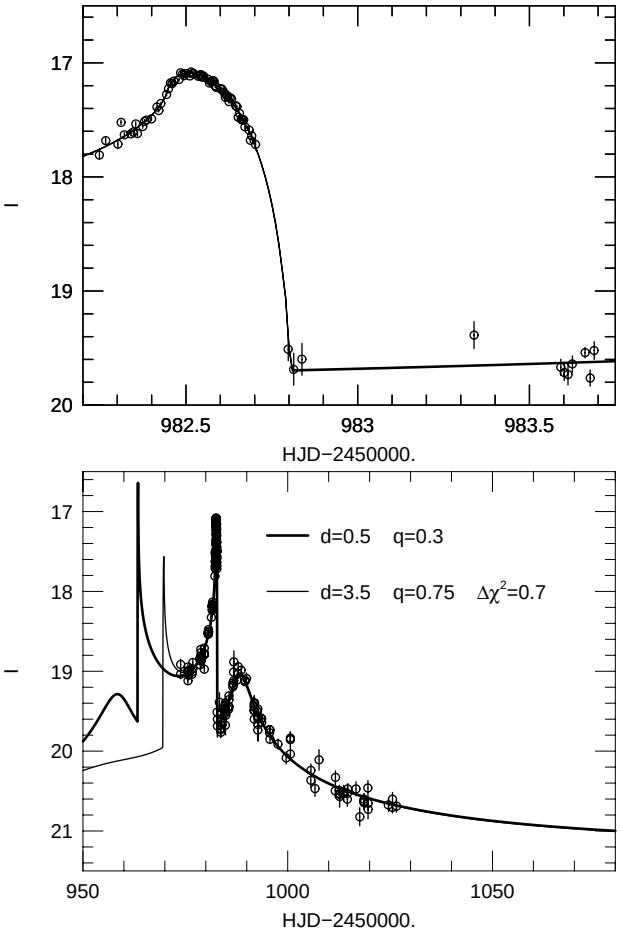

FIG. 7.—PLANET data for MACHO-98-SMC-1 together with two fits both taken from Table 2. In the lower panel, which shows the full light curves, the bold curve is for $(d, q) = (0.5, 0.3)$ and the solid curve is for $(d, q) = (3.5, 0.75)$. In the upper panel, which shows only the caustic crossing region, the two curves are indistinguishable. The SAAO data are shown at the instrumental magnitudes (as reported on the PLANET web site). The data from the remaining three observatories are adjusted in flux by the difference in the best fit to background flux between that observatory and SAAO. See text for details. The $(d, q) = (0.5, 0.3)$ solution gives the nominal "best fit," but the $(d, q) = (3.5, 0.75)$ solution is worse by only $\Delta\chi^2 = 0.7$. That is, the two curves hardly differ over the region where there are data, even though they differ drastically at earlier times.

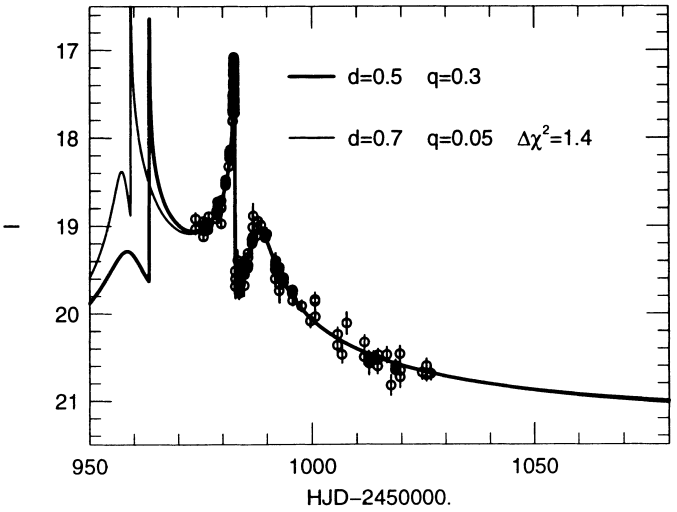

FIG. 8.—PLANET data for MACHO-98-SMC-1 with fits taken from Table 2 for $(d, q) = (0.5, 0.3)$ and $(d, q) = (0.7, 0.05)$. Similar to the lower panel of Fig. 7, except that $\Delta\chi^2 = 1.4$. A close-up view of the caustic crossing is not shown, since it looks identical to the upper panel of Fig. 7.

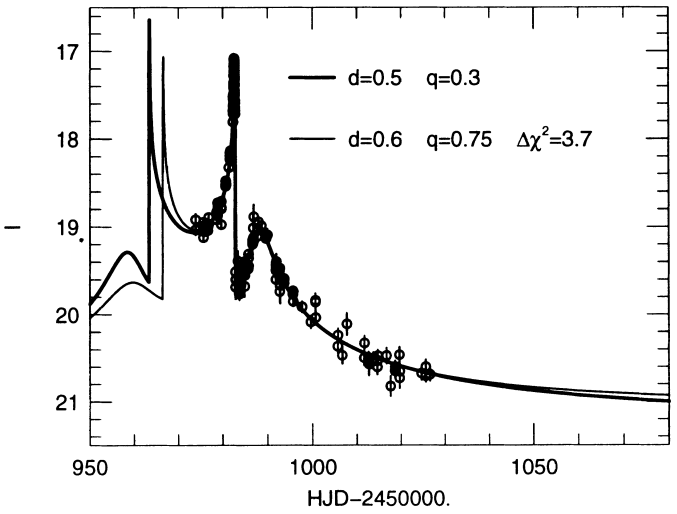

FIG. 9.—PLANET data for MACHO-98-SMC-1 with fits taken from Table 2 for $(d, q) = (0.5, 0.3)$ and $(d, q) = (0.6, 0.75)$. Similar to the lower panel of Fig. 7, except that $\Delta\chi^2 = 3.7$. Note that in this case, in contrast to the previous two, the curves deviate significantly at late times. No close-up view of the caustic crossing is shown because it is identical to the upper panel of Fig. 7.

It is interesting to examine the relation between the two solutions with the same (d, q). From Table 2 one finds that these generally have similar timescales t_E and angles α that differ by approximately 180°. However, the caustic crossing angles ϕ can be quite different. (Since $\sin\phi = t_*/\Delta t$, and Δt is essentially identical for all solutions, $\sin\phi \propto t_*$.) For $d < 1$, these differences are severe for a small value of q and diminish at $q \to 1$. This behavior can be understood by examining Figure 2: since α changes by about 180° and u_0 remains similar for the two solutions, the trajectory followed in the second solution is roughly the reverse of the first. For $q \to 1$, the caustic becomes symmetric, so the angles of the first and second caustic crossings become the same. For q different from 1 (e.g., $q = 0.3$ as in Fig. 2) the caustic is asymmetric, so the two angles are different. This reasoning does not apply to the $d = 3.5$ solutions because the trajectories are not approximately time reversals of each other.

Rhie et al. (1999) note that various fits to the light curve can differ widely on the value of the peak magnification. Specifically, they compare $A_{max} \sim 70$ for their own fit as well as that of Alcock et al. (1999) with $A_{max} \sim 100$ for model I from Albrow et al. (1999a). The peak flux is directly observed (see, e.g., Figs. 5 and 7), so A_{max} depends only on the value of F_s. From Table 2 we see that F_s varies from $0.065F_{20}$ to $0.230F_{20}$, with a nominal best fit at $0.106F_{20}$. The peak magnifications for these three values are, respectively, $A_{max} = 220$, 62, and 135.

5. ADDITIONAL OBSERVATIONS TO BREAK MODEL DEGENERACIES

Since the PLANET data set covers only a portion of the light curve (albeit very well), one might well ask what additional observations would be required to break the degeneracies presented in Table 2. The light curves of the fits at each (d, q) differ substantially in the regions not covered by the data, so it might appear that even data of modest quality in these regions would be adequate to distinguish among the various models. However, it is possible that for a given (d, q) there are other models in which the first caustic is at a different time, or the baseline flux has a different value, and while not the absolute "best" fit to the PLANET data, are still compatible with it. If this is the case, then additional data may leave the degeneracies essentially intact.

We therefore explore three examples of additional data that typically might be available: a precise measurement of the baseline, moderately good coverage of the first caustic, and lower quality coverage of the full light curve (including the early part) but that misses the first caustic.

To investigate the role of additional data, we will assume that our "best fit" $(d, q, \alpha) = (0.5, 0.3, 177°)$ is in fact the true geometry. We emphasize that our data cannot in fact distinguish between the various solutions shown in Table 2. We make this assumption solely for the purpose of exploring the value of additional data.

5.1. *Baseline*

A year (or certainly two) after the caustic crossing, the event will be over and a precise measurement of the baseline can be made. For definiteness, we will assume that this measurement is accurate to 1% and is taken when the event has ended. Inspection of Table 2 shows that I_{base} varies by more than 0.2 mag for the various allowed solutions.

If we add an additional baseline measurement and repeat the entire search procedure, many solutions are eliminated but 27 remain, including examples from all three regions. In particular, all combinations of $d = (0.4, 3.5)$ and $q = (0.3, 0.5, 0.75, 1.0)$ are allowed, as well as $(d, q) = (0.6, 0.1)$, $(0.7, 0.1)$, and $(0.7, 0.05)$ and various combinations of $d = (0.5, 0.6, 2.5, 3.0)$ with $q = (0.3, 0.5, 0.75, 1.0)$. Among these solutions, t_E varies in the range 100 to 227 days and t_* varies in the range 0.90 to 3.42 hr. A broad range of solutions survives partly because many of the original solutions had baselines close to that of the "best fit" and so were not affected by the addition of a baseline "measurement." However, a number of (d, q) pairs whose solutions shown in Table 2 would be ruled out at the 7 σ level by a baseline measurement have alternative solutions that nevertheless manage to meet the baseline constraint. This is not true of all solutions. For example, the solution $(d, q) = (0.6, 0.75)$, which is shown in Figure 9, did not survive the addition of a baseline measurement.

The broad degeneracy in the space of solutions, even with the addition of a precise baseline measurement, confirms the conclusion drawn at the end of § 4, that it is impossible to predict the time of the second caustic crossing from detailed observations of the "first half" of the light curve.

5.2. *First Caustic Crossing*

If the event were alerted before the first caustic crossing, this caustic might be reasonably well covered as a result of routine monitoring by follow-up teams. In this case they might notice the crossing and begin monitoring more intensively. Nevertheless, it is instructive to ask how well simple follow-up monitoring (i.e., without the extra observations triggered by an anomaly alert) over the first caustic crossing would do at resolving the degeneracies seen in Table 2. To be specific, we assume that a total of 5 measurements are made at equal intervals between $t_{cc,1} - 0.2$ days to $t_{cc,1} + 0.2$ days and that these have precision similar to the SAAO data at similar magnitudes, i.e., errors of 7%, 7%, 1.0%, 1.5%, and 2%. Scaling from the error estimates in equation (25) derived from 74 data points, these data should

be sufficient to fix the time of the first caustic crossing to ~ 1 hr. In contrast, the curves shown in Figures 7–9 differ in their times of first caustic crossing by several days. In addition these few measurements also strongly constrain the first caustic crossing time (analogous to Δt) and the scale of the first caustic (analogous to Q). We find that these few data points are sufficient to exclude all solutions found in § 4, except the assumed "true" solution $(d, q) = (0.5,0.3)$.

We argued in § 4.1 that the grid sampling was sufficiently fine because χ^2 was approximately flat over large contiguous regions of the grid. In the present case, one point on the grid has significantly lower χ^2 than all others, so this argument fails. However, at least for the region $d < 1$, the sampling is still adequate to find an approximate local minimum which could then act as a starting point to find the actual local minimum (as described in the first paragraph of § 4.1). On the other hand, because of the generic nature of the $d \leftrightarrow d^{-1}$ degeneracy (Dominik 1999b), one should be cautious about claiming that there are no $d > 1$ solutions simply because there are none on the grid. To truly rule this out, it would be necessary to search on a much finer grid where the grid spacing was set by the range of (d, q) values around the minimum at $(d, q) \sim (0.5,0.3)$ for which $\Delta\chi^2 \lesssim 1$. Since we have not conducted such a search, we cannot absolutely rule out the possibility that a $d > 1$ solution survives the addition of data from the first caustic.

5.3. *Constant Coverage*

Next we assume that the event was covered by routine survey monitoring, once every other day (to allow for weather) for 1000 days before the second crossing and continuing until the end of the PLANET observations on day 1026. In order to complement the investigation in § 5.2, we assume that no observations were taken within 2 days of either caustic crossing. However, to take account of the fact that survey data are usually taken in nonstandard bands, we add two extra parameters to the fit, F_s and F_b for the survey observations. We assume 20% errors at baseline and that the errors scale inversely as the square root of the flux.

Formally we find that only two solutions survive in addition to the "true solution" at $(d, q) = (0.5, 0.3)$, both in its immediate neighborhood at (0.5, 0.5) and (0.6, 0.3). However we also find a cluster of spurious solutions centered at $(d, q) = (3.5,1)$ which has $\Delta\chi^2 = 8.5$. While it might be possible to formally rule out such a solution in this particular case, this low value of $\Delta\chi^2$ suggests that additional data of this type may often leave some degeneracies intact.

5.4. *Summary*

In brief, excellent coverage of a single fold caustic is not sufficient to uniquely determine the parameters of the binary lens, even with the addition of a good late-time baseline measurement. On the other hand, a few measurements over the other caustic can break the degeneracy completely. This degeneracy implies that observations of the first caustic crossing alone cannot be used to reliably predict the time of the second crossing. The addition of survey-type data (infrequent sampling with large errors but covering the whole light curve, even if the caustics are missed) can certainly lift some of the degeneracies, but may leave the $d \leftrightarrow d^{-1}$ degeneracy intact.

This work was supported by grants AST 97-27520 and AST 95-30619 from the NSF, by grant NAG 5-7589 from NASA, by a grant from the Dutch ASTRON foundation through ASTRON 781.76.018, and by a Marie Curie Fellowship from the European Union.

APPENDIX A

RELATION OF MIDPOINT AND CENTER-OF-MASS SYSTEMS

In this paper, we use a coordinate system that has the midpoint of the binary components at the origin. Another widely used system places the origin at the binary center of mass. Since we have the heavier component to the right, the center-of-mass origin lies

$$\Delta = \left(\frac{1-q}{1+q}\right)\frac{d}{2}, \tag{A1}$$

to the *right* of the midpoint origin. Hence, to go from midpoint (m) coordinates to center-of-mass (cm) coordinates, one should apply the transformations

$$u_0^{\rm cm} = u_0^m + \Delta \sin\alpha\,, \quad t_0^{\rm cm} = t_0^m + \Delta t_{\rm E} \cos\alpha\,, \quad u_{x,\rm cc}^{\rm cm} = u_{x,\rm cc}^m - \Delta\,. \tag{A2}$$

Equation (A2) is always an algebraically valid parameterization, but if $u_0^{\rm cm} < 0$, then it violates our convention that the lens system lies on the right-hand side of the moving source. In this case, to maintain this convention, one should apply the further transformation,

$$u_0^{\rm cm} \rightarrow -u_0^{\rm cm}\,, \quad \alpha \rightarrow 2\pi - \alpha\,, \quad u_{y,\rm cc}^{\rm cm} \rightarrow -u_{y,\rm cc}^{\rm cm}\,, \qquad (u_0^{\rm cm} < 0)\,. \tag{A3}$$

APPENDIX B

LIMB-DARKENING FORMALISM

It is possible to parameterize limb darkening in various ways, and Rhie (1999) has evaluated the magnification curve over the caustic crossing for several of these (see her Fig. 4).

One parameterization is

$$S(\theta) = \frac{F_s}{\pi\theta_*^2}\left\{1 - \Gamma\left[1 - \frac{3}{2}\left(1 - \frac{\theta^2}{\theta_*^2}\right)^{1/2}\right]\right\}, \tag{B1}$$

where S is the surface brightness as a function of angular position θ and Γ is the limb-darkening parameter. Note that with this formulation, there is no net flux in the Γ term, so F_s remains the total flux. Convolving the Γ term with the square root singularity of the caustic, we find that the limb-darkened magnification is

$$A(\boldsymbol{u}_p) = A^{\rm fs}(\boldsymbol{u}_p) + \Gamma A^{\rm ld}(\boldsymbol{u}_p)\,, \tag{B2}$$

where $A^{\rm fs}$ is the finite source magnification given by equation (28),

$$A^{\rm ld}(\boldsymbol{u}_p) = A_2^0(\boldsymbol{u}_q)\left(\frac{\Delta u_{q,\perp}}{\rho_*}\right)^{1/2} H_{1/2}\left(-\frac{\Delta u_{p,\perp}}{\rho_*}\right), \tag{B3}$$

$H_n(\eta) \equiv G_n(\eta) - G_0(\eta)$, and

$$G_n(\eta) \equiv \pi^{-1/2}\,\frac{(n+1)!}{(n+1/2)!}\int_{\max(\eta,-1)}^{1}\frac{(1-x^2)^{n+1/2}}{(x-\eta)^{1/2}}\,dx\;\Theta(1-\eta)\,. \tag{B4}$$

Explicitly,

$$G_{1/2}(\eta) = \tfrac{2}{5}\sum_{\epsilon=\pm 1}(3 - 2\epsilon\eta)(\epsilon - \eta)^{3/2}\Theta(\epsilon - \eta)\,. \tag{B5}$$

Equation (13) is then replaced by

$$F(t) = \left(\frac{Q}{\Delta t}\right)^{1/2}\left[G_0\left(\frac{t - t_{\rm cc}}{\Delta t}\right) + \Gamma H_{1/2}\left(\frac{t - t_{\rm cc}}{\Delta t}\right)\right] + F_{\rm cc} + \tilde{\omega}(t - t_{\rm cc})\,. \tag{B6}$$

REFERENCES

Afonso, C., et al. 1998, A&A, 337, L17
———. 1999, in preparation
Albrow, M., et al. 1998, ApJ, 509, 687
———. 1999a, ApJ, 512, 672
———. 1999b, ApJ, 522, 1011
Alcock, C., et al. 1997a, ApJ, 486, 697
———. 1997b, ApJ, 491, 436
———. 1999, ApJ, submitted (astro-ph/9807163)
Aubourg, E., et al. 1993, Nature, 365, 623
Bennett, D. P., & Rhie S. H. 1996, ApJ, 472, 660
Di Stefano, R., & Perna, R. 1997, ApJ, 488, 55
Dominik, M. 1998, A&A, 333, L79
———. 1999a, A&A, 341, 943
———. 1999b, A&A, submitted
Gaudi, B. S., & Gould, A. 1997, ApJ, 486, 85
Gaudi, B. S., & Sackett P. D. 1999, ApJ, submitted
Gould, A. 1995, ApJ, 441, 77
Gould, A., & Andronov, N. 1999, ApJ, 516, 236
Gould, A., & Gaucherel, C. 1997, ApJ, 477, 580
Hardy, S. J., & Walker, M. A. 1995, MNRAS, 276, L79
Kayser, R., & Schramm, T. 1998, A&A, 191, 39
Lennon, D. J., Mao, S., Fuhrmann, K., & Gehren, T. 1996, ApJ, 471, L23
Mao, S., & Paczyński, B. 1991, ApJ, 374, L37
Mao, S., & Di Stefano, R. 1995, ApJ, 440 22
Mao, S., et al. 1994, BAAS, 185, 1705
Rhie, S. H. 1999, in Proc. 2d Int. Workshop on the Identification of Dark Matter, in press (astro-ph 9903024)
Rhie, S. H., Becker, A. C., Bennett, D. P., Fragile, P. C., Johnson, B. R., King, L. J., Peterson, B. A., & Quinn, J. 1999, ApJ, 522, 1037
Sahu, K. C. 1994, Nature, 370, 275
Schneider, P., Ehlers, J., & Falco, E. E. 1992, Gravitational Lenses (Berlin: Springer)
Schneider, P., & Wagoner, R. V. 1987, ApJ, 314, 154
Schneider, P., & Weiss, A. 1986a, A&A, 164, 237
———. 1986b, A&A, 171, 49
Udalski, A., Szymański, M., Mao, S., Di Stefano, R., Kaluzny, J., Kubiak, M., Mateo, M., & Krzemiński, W. 1994, ApJ, 436, L103
Udalski, A., Szymański, M., Pietrzyński, G., Kubiak, M., Woźniak, P., & Żebruń, K. 1998, Acta Astron., 48, 431
Wambsganss, J. 1997, MNRAS, 284, 172
Witt, H. 1990, A&A, 236, 311